AIP Advances

Bi aliovalent substitution in $Li_7La_3Zr_2O_{12}$ garnets: Structural and ionic conductivity effects

Cite as: AIP Advances **10**, 035204 (2020); https://doi.org/10.1063/1.5141764
Submitted: 09 December 2019 . Accepted: 11 February 2020 . Published Online: 02 March 2020

Derek K. Schwanz, Andres Villa, Mahalingam Balasubramanian, Benjamin Helfrecht, and Ernesto E. Marinero

Bi aliovalent substitution in $Li_7La_3Zr_2O_{12}$ garnets: Structural and ionic conductivity effects

Cite as: AIP Advances 10, 035204 (2020); doi: 10.1063/1.5141764
Submitted: 9 December 2019 • Accepted: 11 February 2020 •
Published Online: 2 March 2020

Derek K. Schwanz,[1] Andres Villa,[1] Mahalingam Balasubramanian,[2] Benjamin Helfrecht,[1] and Ernesto E. Marinero[1,a)]

AFFILIATIONS

[1]School of Materials Engineering, Purdue University, West Lafayette, Indiana 47907, USA
[2]Advanced Photon Source, Argonne National Laboratory, Argonne, Illinois 60439, USA

[a)]**Author to whom correspondence should be addressed:** eemarinero@purdue.edu

ABSTRACT

We report on the synthesis of cubic-phase garnet-type solid-state electrolytes based on Bi-doped $Li_7La_3Zr_2O_{12}$ (LLZO). Bi aliovalent substitution of Zr in LLZO utilizing the Pechini processing method is employed to synthesize $Li_{7-x}La_3Zr_{2-x}Bi_xO_{12}$ compounds. A strong dependence of the ionic conductivity on Bi content is observed, and under our synthesis and sintering conditions, a >100-fold increase over the un-doped sample is observed for x=0.75. Cubic-phase $Li_6La_3Zr_1BiO_{12}$ compounds are generated upon annealing in air in the temperature range 650 °C–900 °C. In contrast, in the absence of Bi, the cubic garnet phase of $Li_7La_3Zr_2O_{12}$ is not formed below 700 °C and a transformation to the tetragonal phase is observed at ~900 °C for this un-doped compound. The role of Bi in lowering the formation temperature of the garnet cubic phase and in the ionic conductivity improvements is investigated in this work. We ascribe the effect of Bi-doping on ionic conductivity increments to changes in Li^+-site occupancy and lattice parameters and the reduction in the formation temperature for the cubic-phase formation to rate enhancements of the solid-state reaction. To identify the site occupancy of Bi in the garnet structure, we employ synchrotron extended x-ray absorption fine structure spectroscopy. Our results indicate that Bi additions occupy the Zr-type sites exclusively, to within the accuracy of the measurements.

INTRODUCTION

Conventional liquid electrolyte–salt combinations in lithium batteries present inherent safety concerns due to dendritic growth and thermal runaway issues.[1,2] Solid-state electrolytes provide increased functionality to the cell in terms of enhanced stability, cyclability, and safety.[3–5] However, ionic conductivity through solid electrolyte materials is in general orders of magnitude lower than that in liquid electrolytes.[6] If the ionic conductivity of lithium-ion conducting solid materials can be significantly increased, battery safety and performance can be improved significantly. $Li_7La_3Zr_2O_{12}$ (LLZO) garnet-type oxides have been shown to be promising materials for electrolyte applications on account of their relatively high ionic conductivity and good chemical stability.[7–10] Room temperature LLZO exists as two high-temperature stabilized polymorphs: an ordered, low ionic conductivity I41/acdZ tetragonal phase and a more disordered, high ionic conductivity Ia-3d cubic phase.[11–14]

BACKGROUND

Optimization of the Li^+-site occupancy and lattice parameter modifications of LLZO has been attributed to reported improvements of ionic conductivity in this garnet structure.[15–18] However, high-temperature heat treatments were originally employed to achieve the cubic-phase stabilization and densification required for electrolyte applications.[7] Subsequently, site-specific aliovalent doping has proven to be an effective approach for reducing the temperature stabilization of the garnet cubic phase.[19] Dopants have also been used to modify the Li^+ content in LLZO through atomic substitution onto the 24c and 16a sites of the La^{3+} and Zr^{4+} ions, respectively.[9,20–26] These aliovalent dopants modify also the geometry of the Li^+ conduction channels.[16,25,26] Such studies confirm that there is an optimized Li^+ occupancy ratio providing the highest ionic conductivity.[27–29] The cubic garnet lattice has a maximum of 7.5 Li^+ sites per formula unit, and an optimized ionic conductivity has been

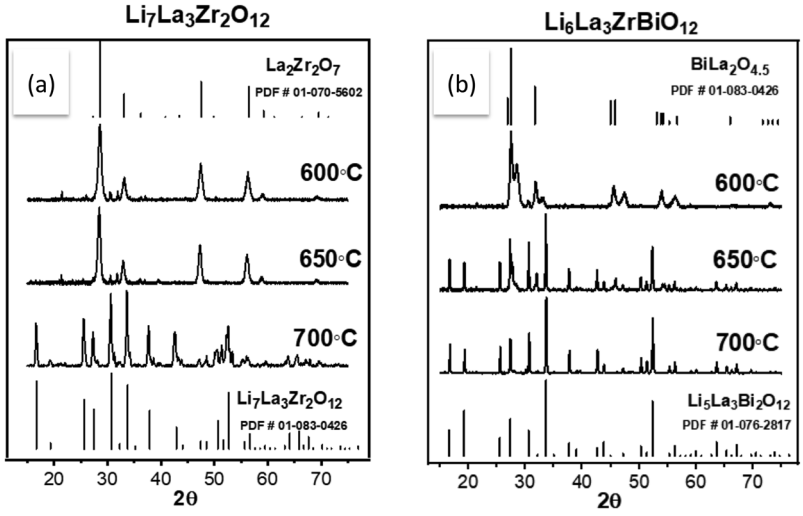

FIG. 1. X-ray diffraction spectra for (a) $Li_7La_3Zr_2O_{12}$ and (b) $Li_6La_3Zr_1BiO_{12}$ samples calcined at 600 °C, 650 °C, and 700 °C. Figure 1(a) shows that at 700 °C, the un-doped sample exhibits multiple phases. In contrast, Fig. 1(b) indicates that Bi-doped LLZO converts to the cubic phase at 650 °C, with only trace amounts $BiLa_2O_{4.5}$ observable. At 700 °C, the doped sample exhibits the pure cubic phase. Reference PDF spectra are provided to identify the crystal structures formed.

determined to lie near a Li^+ stoichiometry of 6.5.[30] Thus, dopants simultaneously modify the lattice spacing and the Li^+ stoichiometry, resulting in large changes in the lithium-ion transport throughout the garnet structure.

The mechano-chemical synthesis of LLZO from oxide precursors without dopants can require as much as 36 h of ball-milling time at 1230 °C for stabilization of the cubic phase.[7] Sol–gel synthesis, such as the Pechini method, enables more efficient homogeneous mixing of the precursor materials, thereby enhancing the reaction kinetics for LLZO formation.[22,31,32] Therefore, in this work, we use the Pechini method to decrease both the time and temperature needed for synthesizing cubic-phase $Li_{7-x}La_3Zr_{2-x}Bi_xO_{12}$ (LLZBO) compounds.

We note that an ideal dopant should simultaneously decrease the activation barrier for compound formation while aiding densification during powder sintering. Here, we investigate Bi-aliovalent doping on the 16c Zr site in $Li_{7-x}La_3Zr_{2-x}Bi_xO_{12}$ garnet oxides. Bi has been shown to be useful in both mechano-chemical and solution based synthesis of high ionic conductivity garnets due to its large ionic radius and Bi^{5+} valence.[31,33] In this work, we also report on the effect of Bi-doping on explosive crystalline grain growth as a function of Bi content under isothermal conditions.

EXPERIMENTAL PROCEDURE

Garnet oxides of the nominal composition $Li_{7-x}La_3Zr_{2-x}Bi_xO_{12}$ were fabricated from nitrate precursors by the citrate-gel Pechini method using a polymerized complex intermediary. The full synthesis method is provided in the supplementary material. To study dopant effects on phase evolution, polymerized complexes with the composition $Li_{7-x}La_3Zr_{2-x}Bi_xO_{12}$ (x = 0, 0.25, 0.5, 0.75, and 1.0) were calcined between 600 °C and 700 °C for 10 h in an MgO crucible.[34,35] X-ray diffraction was employed to determine the role of Bi in the formation of the cubic phase and in the phase stability as a function of garnet composition. A Bruker D8 Focus apparatus equipped with a Cu K alpha source (1.54 Å) with a scan rate of 5°/min was employed. Figures 1(a) and 1(b) show diffraction patterns for $Li_7La_3Zr_2O_{12}$ and $Li_6La_3ZrBiO_{12}$, respectively, powders calcined at 600 °C, 650 °C, and 700 °C.

Extended X-ray Absorption Fine Structure (EXAFS) was employed to investigate the site occupancy of Bi in the garnet crystalline structure. EXAFS measurements were carried out at the L_3-edges of Bi and La and the K-edge of Zr at beamline 20-BM at the Advanced Photon Source at Argonne National Laboratory.

To evaluate the effects of Bi-doping on LLZO's microstructure and ionic conductivity, pellets were fabricated with different Bi contents (x = 0, 0.25, 0.5, 0.75, and 1.0) from sintered precursor powders (see the supplementary material). Pellet fractured surfaces were examined with scanning electron microscopy (SEM, FEI XL40) to compare their microstructure [Figs. 3(a)–3(d)]. Relative density measurements were derived employing the Archimedes method.

To measure the ionic conductivity of the pellets, we employed Electrochemical Impedance Spectroscopy (EIS) in the frequency

TABLE I. Summary of pellet dimensions and physical properties for Bi-doped LLZO pellets sintered at 900 °C for 10 h.

Composition	Bi	Thickness (mm)	Density (g/cm^3)	Relative density	Ionic conductivity (S/cm) at 27 °C
$Li_7La_3Zr_2O_{12}$	0	1.51	4.0	0.79	Not measurable
$Li_{6.75}La_3Zr_{1.75}Bi_{0.25}O_{12}$	0.25	1.48	4.2	0.80	5.0×10^{-6}
$Li_{6.5}La_3Zr_{1.5}Bi_{0.5}O_{12}$	0.5	1.30	4.4	0.81	7.2×10^{-6}
$Li_{6.25}La_3Zr_{1.25}Bi_{0.75}O_{12}$	0.75	1.01	4.7	0.83	2.0×10^{-4}
$Li_6La_3ZrBiO_{12}$	1.0	1.08	4.8	0.84	1.2×10^{-5}

range of 0.0001 Hz–300 kHz employing a Solartron SI 1260 impedance/gain-phase analyzer together with a SI 1287 electrochemical interface. Complex impedance plots used to obtain ionic conductivity are provided in Fig. 3(e) and in Table I; ionic conductivity measurements for LLZBO samples with various Bi contents are provided. Measurements were taken at 27 °C and the results were analyzed using equivalent circuits models as described by Huggins.[36]

RESULTS AND DISCUSSION

In Fig. 1, we compare the transformation from a $La_2Zr_2O_7$ pyrochore-type phase into an Ia-3d garnet cubic phase for both the un-doped and Bi-doped LiLaZrO samples in the temperature range 600 °C–700 °C, whereas as seen in Fig. 1(b), the formation of the cubic phase is clearly evident for the LiLaZrBiO sample at 650 °C, with only trace amounts of $BiLa_2O_{4.5}$ present. In contrast, the un-doped LiLaZrO sample requires a temperature >700 °C to transform into the desired cubic phase. As Fig. 1(a) indicates, at 700 °C, the XRD spectrum for LLZO reveals multiple phases present. Kokal *et al.*[22] employed sol–gel synthesis of LLZO and observed the formation of the cubic phase at 708 °C.

$Li_6La_3Zr_1BiO_{12}$ [Fig. 1(b)] transforms almost 100% into the garnet cubic phase at around 650 °C, with only trace amounts of $BiLa_2O_{4.5}$ present. This doped sample forms a mixture of $La_2Zr_2O_7$ along with R-3mH $BiLa_2O_{4.5}$ when heat-treated at 600 °C and readily starts to convert to the cubic garnet phase at 650 °C, a lower temperature than for $L_7L_3Z_2O_{12}$. In contrast, the $La_2Zr_2O_7$ precursor phase is still mainly present at 650 °C for the case of LLZO, as seen in Fig. 1(a).

Representative raw EXAFS spectra are shown in Fig. 2(a). The structural parameters of the dominant pair correlations, extracted from fits to the data at the various edges, are provided in supplementary material Table I. For $Li_6La_3Zr_1BiO_{12}$, the Bi local environment is consistent with Bi atoms occupying Zr-type sites. Bi is surrounded by ~ 6 oxygen and ~6 lanthanum atoms at 2.097 ± 0.007 Å and 3.656 ± 0.014 Å. The data can be fit remarkably well by considering only the occupancy of Zr-type sites; this is illustrated in Fig. 2(b). There is no clear evidence for the presence of longer Bi–O or Bi–Zr/Bi correlations at distances expected for Bi occupying La-type sites with a 3 + valence. We, therefore, infer that Bi additions occupy the Zr-type sites exclusively, to within the accuracy of the measurements. The structural parameters, reported in supplementary material Table I, reveal local distortions around the Zr and La sites to accommodate Bi additions. Furthermore, there is an increase in the mean-squared relative displacement for many correlations, pointing to an increase in static disorder.

SEM analysis reveals drastic differences in the microstructure as a function of Bi content. The pure LLZO pellet, as seen in Fig. 3(a), exhibits sub-micrometer sized particles and almost no inter-particle coalescence, indicating that very little sintering occurs at 900 °C. In contrast, Figs. 3(b)–3(d) show significant grain growth and evidence of sintering. The sample with the highest amount of Bi [Fig. 3(d)] shows the largest grain growth and a higher degree of inter-particle coalescence. Bi additions to LLZO have a remarkable impact on grain growth. Such a large enhancement in grain growth could be ascribed to the plausible formation of a liquidus phase at 900 °C, as the $Bi_2O_3 + ZrO_2$ system is reported[37] to exhibit such a phase at temperatures of ~830 °C. The presence of a liquidus phase would dramatically increase diffusion and crystallization kinetics, accounting for the explosive grain growth observed in our work with increasing Bi-doping. We note that Wang and Sakamoto[38] report that Bi-doping of LLZO results in a dramatic decrease in densification temperature.

With reference to Fig. 3(e), the tail on the low frequency spectrum indicates the capacitive nature of the ion-blocking electrodes, while the semicircles at the high frequency end correspond to the resistive-capacitive response of the bulk material. The semicircles at high frequencies are somewhat compressed, indicating separate contributions from both the bulk and grain boundaries, but there is no significant separation. As there is no clear separation between the bulk and grain boundaries, the more resistive nature of the

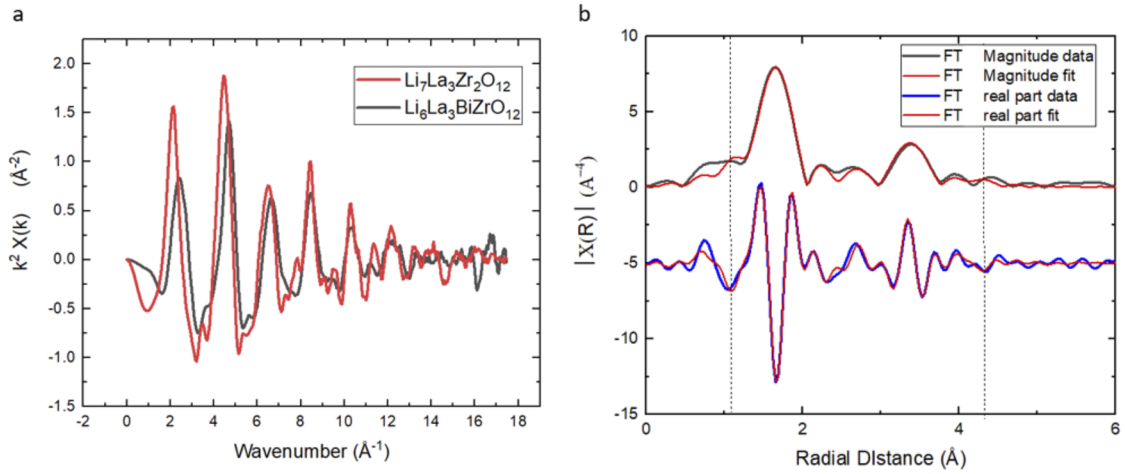

FIG. 2. (a) Representative EXAFS measurements at the Bi L_3-edge (black) and Zr K-edge (red) and (b) corresponding Fourier transform for the magnitude and real portion of the Bi EXAFS data and associated fitting using Demeter software. Dotted vertical lines indicate the range covered by the fit.

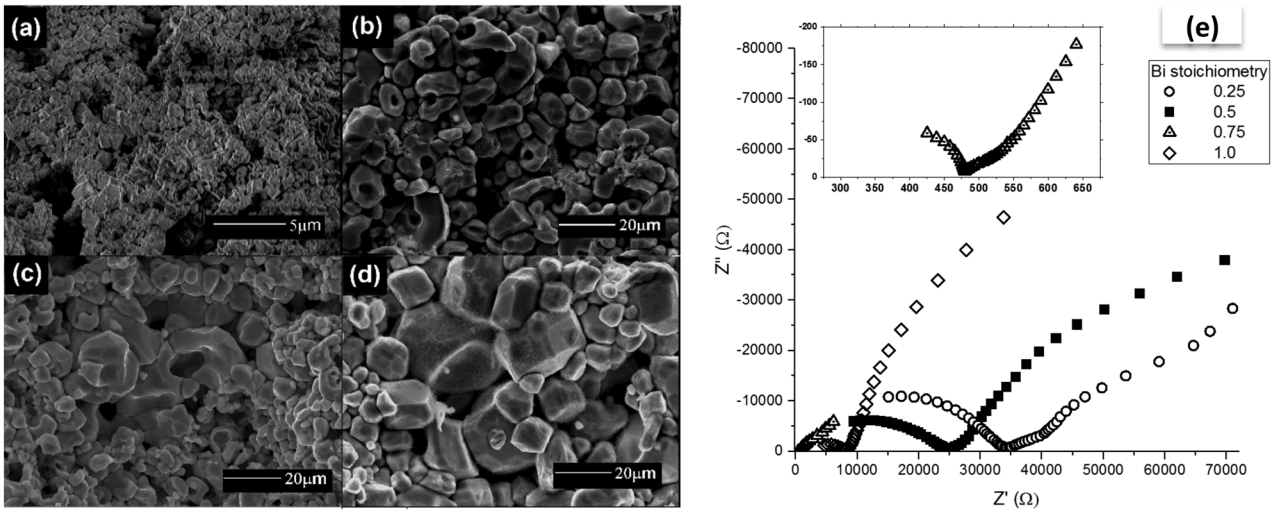

FIG. 3. Doped LLZO microstructure and AC impedance measurements. (a)–(d) SEM images of pellet fracture surfaces for garnet oxides sintered at 900 °C for 10 h. The sample stoichiometries are as follows: (a) $Li_7La_3Zr_2O_{12}$, (b) $Li_{6.5}La_3Zr_{1.5}Bi_{0.5}O_{12}$, (c) $Li_{6.25}La_3Zr_{1.25}Bi_{0.75}O_{12}$, and (d) $Li_6La_3ZrBiO_{12}$. To facilitate comparison of grain size, the image magnification of (a) is ~4x higher than for (b)–(d). (e) Nyquist plots for pellet samples with Bi = 0.25, 0.5, 0.75, and 1.0; the inset corresponds to Bi = 0.75 at frequencies below 700 Hz.

bulk dominates the behavior in comparison to that of the grain boundaries. The compressed semicircles allow for the measurement of the total resistance, as extracted from the low frequency intercept of the Z′(Ω) axis, as done in similar studies reported in Ref. 14. Measurements of the $Li_7La_3Zr_2O_{12}$ sample were hindered by its inferior densification at the sintering temperature (900 °C), resulting in lack of interconnectivity, as indicated in Fig. 3(a). The Bi containing samples yield ionic conductivity ranging from 10^{-6} to 10^{-4} S/cm, and the results are summarized in Table I along with other pellet sample physical properties. As noted in Table I, at the sintering temperatures employed, the pellets are not fully densified. This can be expected to reduce the maximum ionic conductivity attainable in our samples. In fact, reported measurements for LLZO typically utilize higher sintering temperatures (>1000 °C) or the addition of sintering aids to enhance densification.[7,13,22,23] Xia *et al.*[39] added Al_2O_3 to $Li_{6.8}La_3Zr_{1.8}Bi_{0.2}O_{12}$ and used a sintering temperature of 1100 °C to enhance densification to improve ionic conductivity in LLZBO. They report an ionic conductivity value of 6.3×10^{-5} S/cm, which compares favorably to that measured in our experiments (5.0×10^{-6} S/cm) for $Li_{6.75}La_3Zr_{1.75}Bi_{0.25}O_{12}$ (sintered at 900 °C without added sintering agents).

The increment of the ionic conductivity with increasing amounts of Bi can be partially ascribed to enhanced grain growth, as evidenced in Fig. 3, and to higher densification, as revealed by Archimedes measurements of relative density, as summarized in Table I. Additionally, the increased inter-particle connectivity and coalescence observed in Fig. 3 results in lower resistance to ionic transport through the garnet structure. Thus, samples containing lower amounts of Bi such as $Li_{6.75}La_3Zr_{1.75}Bi_{0.25}O_{12}$ can be expected to have a higher resistance due to larger free volume in the structure.

As the Bi stoichiometry is varied, the Li^+ occupancy to vacancy ratio proportionally changes, with each Bi^{5+} creating an additional Li^+ vacancy. Thus, it can be expected that each pellet composition studied exhibits different Li^+ sub-lattice occupancy ratios, resulting in electronic structure changes in $Li_{7-x}La_3Zr_{2-x}Bi_xO_{12}$ as a function of Bi content. $Li_{6.25}La_3Zr_{1.25}Bi_{0.75}O_{12}$ exhibits the highest measured ionic conductivity. This sample corresponds to a Li stoichiometry of 6.25 which is lower than the optimum value of 6.5 reported by Zeier.[30] The difference is likely due to microstructural and densification changes in our samples with varying amounts of Bi. To differentiate structural effects from electronic effects, hot pressing methods are employed in comparing samples with similar densification characteristics.[15,23] In this work, microstructural changes are observed with Bi additions; therefore, both densification and Li^+ occupancy differences likely contribute to the ionic conductivity values reported here.

For the case of $Li_{6.75}La_3Zr_{1.75}Bi_{0.25}O_{12}$ samples sintered at 900 °C for 10 h, there is insufficient thermal activation for full densification; hence, even if the electronic structure for this composition were to be an optimum for ionic transport, the degree of grain interconnectivity is insufficient for optimum ionic transport. Therefore, it is plausible that with higher densification, the maximum ionic conductivity for Bi-doped materials corresponds to a different composition than the one here reported ($Li_{6.25}La_3Zr_{1.25}Bi_{0.75}O_{12}$). Higher ionic conductivities may be attainable in compounds with different Bi contents, utilizing higher sintering temperatures and additives to form denser garnet structures.

CONCLUSIONS

We utilized the sol–gel Pechini method to synthesize, to our knowledge for the first time, Bi-doped cubic LLZO garnets at temperatures of ~650 °C. Whereas similar compounds have been reported by others employing mechano-chemical methods,[38–40]

annealing temperatures in the range of 850 °C–1100 °C were needed to form the cubic phase. A strong dependence of the ionic conductivity on Bi content was observed in this work. A value of 2.0×10^{-4} S/cm was measured for $Li_{6.25}La_3Zr_{1.25}Bi_{0.75}O_{12}$ at 27 °C. In addition to the effect of doping on Li^+-site occupancy, densification strongly influences the ionic conductivity in these solid-state electrolytes. For example, Wang and Sakamoto[38] reported a value of 1.0×10^{-4} S/cm in a sample of $Li_6La_3Zr_1BiO_{12}$ having a relative density of 94%. The same sample composition fabricated in this work, but having a lower relative density of 84%, yielded ~10x lower ionic conductivity (1.2×10^{-5} S/cm).

Whereas the ionic conductivity values reported in this work are comparable to those obtained by doping LLZO with different elements[41–43] (with the exception of Ga-doped LLZO, in which a value of 1.46×10^{-3} S/cm was measured[44]), Bi-doping significantly reduces the temperature needed to form the high ionic conductivity cubic phase. This temperature reduction is not solely due to the synthesis method (Pechini vs mechano-chemical) as comparison with reported results employing sol–gel synthesis of doped-LLZO indicates that Bi additions reduces the cubic-phase formation temperature from 50 °C to 300 °C.[43,45–47] Furthermore, we find that Bi-doping of LLZO results also in explosive grain growth. Furthermore, Wang and Sakamoto[38] observed a dramatic reduction in densification temperature in Bi-doped LLZO. We hypothesize that these microstructural and reaction kinetic changes are likely the result of the formation of low melting point eutectics at our sintering temperatures (900 °C) as the $Bi_2O_3 + ZrO_2$ system is reported to exhibit[37] a liquidus point ~830 °C.

In addition, we have identified, employing EXAFS, that Bi additions occupy the Zr-type sites exclusively, to within the accuracy of the measurements. This is in contrast to first principles computations that predict the site-preference for Bi to be the La site.[48]

In summary, the reduced cubic-phase formation temperature afforded by Bi-doping of LLZO in combination with the sol–gel synthesis method provides a significant reduction in the energetic needs required to fabricate these promising solid-state electrolytes, thereby mitigating one of the key impediments that have been identified for the implementation of these materials into battery technology.[49,50]

SUPPLEMENTARY MATERIAL

Additional experiments on the following are given in the supplementary material: (a) synthesis of Bi-doped LiLaZrBiO garnet materials; (b) thermogravimetric analysis (TGA) to determine polymerized complex decomposition, subsequent oxidation, and the formation of the garnet oxides; (c) structural parameters derived from synchrotron EXAFS measurements; and (d) XRD analysis of the cubic-phase formation of LiLaZrO as a function of Bi composition upon powder sintering at 900 °C for 10 h.

ACKNOWLEDGMENTS

The authors acknowledge support from the Purdue University School of Materials Engineering startup funds for Dr. Marinero and Mexico's Consejo Nacional de Ciencia y Tecnología (CONACYT) for partial support for Andres Villa. The research by M.B. was supported by the Joint Center for Energy Storage Research (JCESR). Sector 20 operations at the Advanced Photon Source are supported by the US Department of Energy (US DOE, Contract No. DE-AC02-06CH11357) and the Canadian Light Source. We also thank Juan Carlos Verduzco, School of Materials Engineering, Purdue University, for a critical reading of this manuscript and valuable suggestions.

REFERENCES

[1] R. Premanand, A. Durairajan, B. Haran, and R. White, J. Electrochem. Soc. **149**(1), A54 (2002).
[2] R. Selim and P. Bro, J. Electrochem. Soc. **121**, 1457 (1974).
[3] V. Thangadurai and W. Weppner, Ionics **8**(3-4), 281 (2002).
[4] J. M. Tarascon and M. Armand, Nature **414**, 359 (2001).
[5] B. Wang, J. B. Bates, F. X. Hart, B. C. Sales, R. A. Zuhr, and J. D. Robertson, J. Electrochem. Soc. **143**(10), 3203 (1996).
[6] P. Knauth, Solid State Ionics **180**, 911 (2009).
[7] R. Murugan, V. Thangadurai, and W. Weppner, Angew. Chem., Int. Ed. **46**, 7778 (2007).
[8] M. Matsui, K. Takahashi, K. Sakamoto, A. Hirano, Y. Takeda, O. Yamamoto, and N. Imanishi, Dalton Trans. **43**, 1019 (2014).
[9] S. Ohta, T. Kobayashi, and T. Asaoka, J. Power Sources **196**, 3342 (2011).
[10] Y. Shimonishi, A. Toda, T. Zhang, A. Hirano, N. Imanishi, O. Yamamoto, and Y. Takeda, Solid State Ionics **183**, 48 (2011).
[11] N. Bernstein, M. Johannes, and K. Hoang, Phys. Rev. Lett. **109**, 205702 (2012).
[12] J. Awaka, A. Takashima, K. Kataoka, N. Kilma, Y. Idemoto, and J. Akimoto, Chem. Lett. **40**(1), 60 (2011).
[13] J. Awaka, N. Kijima, H. Hayakawa, and J. Akimoto, J. Solid State Chem. **182**, 2046 (2009).
[14] J. Wolfenstine, E. Rangasamy, J. L. Allen, and J. Sakamoto, J. Power Sources **208**, 193 (2012).
[15] J. L. Allen, J. Wolfenstine, E. Rangasamy, and J. Sakamoto, J. Power Sources **206**, 315 (2012).
[16] L. J. Miara, S. P. Ong, Y. Mo, W. D. Richards, Y. Park, J. M. Lee, H. S. Lee, and G. Ceder, Chem. Mater. **25**, 3048 (2013).
[17] M. P. O. Callaghan and E. J. Cussen, Chem. Commun. **2007**, 2048.
[18] S. Ramakumar, N. Janani, and R. Murugan, Dalton Trans. **44**, 539 (2015).
[19] L. Dhivya, N. Janani, B. Palanivel, and R. Murugan, AIP Adv. **3**, 082115 (2013).
[20] H. Buschmann, J. Dölle, S. Berendts, A. Kuhn, P. Bottke, M. Wikening, P. Hetjans, A. Senyshyn, H. Ehrenberg, A. Lotnyk, V. Duppel, L. Kienle, and J. Janek, Phys. Chem. Chem. Phys. **13**, 19378 (2011).
[21] C. A. Geiger, A. E. Alekseev, B. Lazic, M. Fisch, T. Armbruster, R. Langer, M. Fechttelkord, N. Kim, T. Pettke, and W. Weppner, Inorg. Chem. **50**(3), 1089 (2011).
[22] I. Kokal, M. Somer, P. H. L. Notten, and H. T. Hintzen, Solid State Ionics **185**(1), 42 (2011).
[23] E. Rangasamy, J. Wolfenstine, and J. Sakamoto, Solid State Ionics **206**, 28 (2012).
[24] V. Thangadurai and W. Weppner, J. Am. Ceram. Soc. **88**(2), 411 (2005).
[25] L. Dhivya and R. Murugan, ACS Appl. Mater. Interfaces **6**(20), 17606 (2014).
[26] Y. Li, J. T. Han, C. A. Wang, and J. B. Goodenough, J. Mater. Chem. **3**, 15357 (2012).
[27] E. J. Cussen, J. Mater. Chem. **20**, 5167 (2010).
[28] S. Mukhopadhyay, T. Thompson, J. Sakamoto, A. Huq, J. Wolfenstine, J. L. Allen, N. Bernstein, D. A. Steward, and M. D. Johannes, Chem. Mater. **27**(10), 3658 (2015).
[29] S. Adams and R. P. Rao, J. Mater. Chem. **22**, 1426 (2012).
[30] W. Zeier, Dalton Trans. **43**, 16133 (2014).
[31] Y. X. Gao, X. P. Wang, W. G. Wang, Z. Zhuang, D. M. Zhang, and Q. F. Fang, Solid State Ionics **181**, 1415 (2010).

[32]M. Kotobuki and M. Koishi, Ceram. Int. **40**(3), 5043 (2014).
[33]R. Murugan, W. Weppner, P. Schmid-Beurmann, and V. Thangadurai, Mater. Sci. Eng., B **143**(1-3), 14 (2007).
[34]D. K. Schwanz and E. E. Marinero, U.S. patent 10,439,250 (10 November 2015).
[35]D. K. Schwanz, *Open Access Theses*, Purdue University, 2016, https://docs.lib.purdue.edu/open_access_theses/999.
[36]R. A. Huggins, Ionics **8**(3-4), 300 (2002).
[37]T. Takamori and M. W. Schafer, J. Am. Ceram. Soc. **73**(5), 1453 (1990).
[38]M. Wang and J. Sakamoto, Ionics **24**, 1861 (2018).
[39]Y. Xia *et al.*, Front. Mater. Sci. **9**(4), 366 (2015).
[40]R. Wagner *et al.*, Inorg. Chem. **55**, 12211 (2016).
[41]S. Song *et al.*, Electrochim. Acta **270**, 501 (2018).
[42]S. Ramakumar *et al.*, Phys. Chem. Chem. Phys. **15**, 11327 (2013).
[43]X. Liu *et al.*, J. Am. Ceram. Soc. **100**(4), 1527 (2017).
[44]J. F. Wu *et al.*, ACS Appl. Mater. Interfaces **9**, 1542 (2017).
[45]N. Rosenkiewitz *et al.*, J. Power Sources **278**, 104 (2015).
[46]X. Zhang and J. W. Fergus, ECS Trans. **72**(7), 133 (2016).
[47]Y. Jin and P. J. McGinn, J. Power Sources **196**(20), 8683 (2011).
[48]L. J. Miara *et al.*, ACS Chem. Mater. **27**, 2040 (2015).
[49]Z. Gao *et al.*, Adv. Mater. **30**(17), e1705702 (2018).
[50]A. Manthiram, X. Yu, and S. Wang, Nat. Rev. Mater. **2**, 16103 (2017).